Article

Optimizing Stainless Steel Bearings: Enhancement of Stainless Steel Bearing Fatigue Life by Low-Temperature Forming

Alexander Heinrich Bodewig * , Florian Pape and Gerhard Poll

Institute for Machine Design and Tribology (IMKT), Leibniz University Hanover, 30823 Garbsen, Germany; pape@imkt.uni-hannover.de (F.P.); poll@imkt.uni-hannover.de (G.P.)
* Correspondence: bodewig@imkt.uni-hannover.de

Abstract: A proposed low-temperature forging method is presented to enhance stainless steel bearings by creating a martensitic subsurface layer, significantly boosting bearing fatigue life due to increased surface hardness. This technique induces beneficial residual stresses, particularly in axial bearings, streamlining their construction and improving machine elements. Challenges persist, especially with radial bearings, but simplicity in axial bearing forging promotes compact, resource-efficient facility construction. Future research will focus on applying this technique to axial bearing washers, potentially replicating success in other bearing components. Despite the energy expenditure on cooling during forging, the substantial increase in bearing fatigue life offsets this, enhancing overall durability and reliability of critical machine components. Integration of this forging technique into bearing fabrication appears seamless, offering a promising trade-off between energy use and enhanced performance.

Keywords: bearings; bearing life; stainless steel; cold forming

1. Introduction

Due to global economic and ecological changes, the usage of innovative environmentally friendly and resource-saving technologies is a focus of current research. In addition to the application of light metals, ultrahigh-strength steel alloys and load-adapted component structures with improved material properties are increasingly being used. By incorporating alloying elements and targeted heat treatment, properties such as hardness, residual stresses, yield strength, tensile strength, elongation at break, toughness, fatigue strength, heat strength, machinability, and corrosion resistance of the steel can be varied in many ways and adapted to requirements. To manufacture highly resilient components, manufacturing processes of forming technology are often used. Besides densification, subsurface compressive residual stresses can be achieved by forging processes. For example, achieving a beneficial subsurface structure forging process has also been a focus in the project "Tailored Forming". Here, a forging process is undertaken after a laser cladding or plasma welding procedure on bearings made of an AISI 52100 raceway on AISI 1022 M structure material or martensitic chromium silicon steel (1.4718) on a base substrate of S235 (1.0038) steel [1,2]. These forming processes could serve to improve surface quality, though the temperature has to be adjusted to enable an adequate forging process. The positive effects of residual compressive stresses on service life in component areas subjected to the highest rolling stresses have been known for a long time [3–5]. Previous studies were able to reveal the beneficial effects of preinduced compressive residual stresses on bearing fatigue life for AISI 52100 bearings. These residual stresses were induced by deep rolling and turn-rolling [6]. In the present study, the optimization of bearings made of stainless steel was the focus. Such bearings are used for application in the food industry and paper industry or for chemical processes as mass products [7], but can also be found in the form of high-strength stainless steel bridge roller bearings [8]. Also, to withstand

high-temperature oxidation and corrosion, aircraft bearings are made of stainless steel [9], the idea being to achieve a beneficial residual stress-state subsurface of the bearing by improved forging processes. In this case, a particular focus must be on a low-temperature forging process. In general, due to hardening during the forging process, forming at low temperatures endows the component with higher material strength. During the forming of metastable austenitic steels, the resulting hardening is significantly increased by an additional deformation-induced martensitic phase transformation (see Figure 1 on the left). The phase transformation is accompanied by the introduction of compressive stresses due to the increase in volume of the martensitic phase.
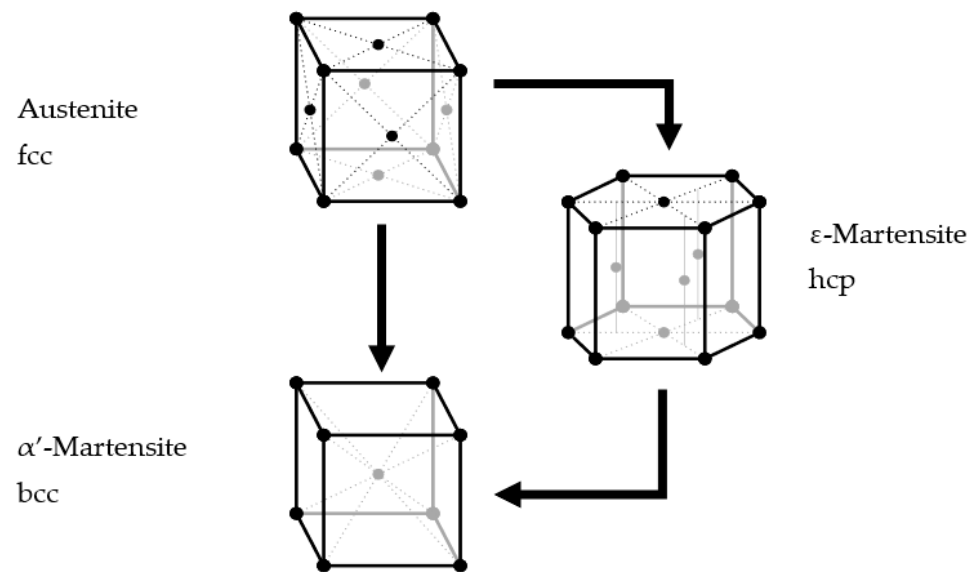

Figure 1. Hardening of metastable austenitic materials according to /Lin00/.

1.1. Martensitic Phase Transformation in Forging

In the cold forming of metastable austenitic steels, in addition to the hardening process, an additional strength-enhancing phase transformation occurs, which is induced by externally introduced stresses and strains. Most stainless austenitic CrNi steels with approximately 18% Cr and 10% Ni are metastable austenitic in the non-deformed state. During forming, a partial conversion of the cubic face-centered (fcc) phase of the austenite into a cubic space-centered (bcc) martensitic phase can take place [10].

Metastable austenitic stainless steels are mainly used in the chemical and food industries, e.g., for condensers, heat exchangers, coolers and pipelines. These are mainly sheet metal components. On the other hand, the effect of deformation-induced martensite formation in the field of cold forming has so far been little used industrially. These stainless steels are well known for applications for excavator bucket teeth and forklift tines, which harden due to mechanical loads in use.

Figure 1 shows the basic deformation-induced transformation process and the resulting hardening. The formed martensite consists of ferritic α'-martensite, which has a tetragonal-distorted fcc structure, and unstable ε-martensite with an hcp structure. This can be converted into α'-martensite (bcc) with further stress [11]. The phase transformation from austenite to martensite caused by deformation is generally referred to as deformation-induced martensite formation.

Furthermore, there is a dependence between deformation-induced martensite formation and the forming temperature. By cooling the samples to T = −5 °C, an increase in the martensite content in excess of experiments conducted at room temperature is possible. An increased forming temperature, on the other hand, reduces the effect of martensitic phase transformation (Figure 2). At a temperature of T = 60 °C, martensite formation is almost

completely suppressed. This temperature dependence has already been described by [12], among others.
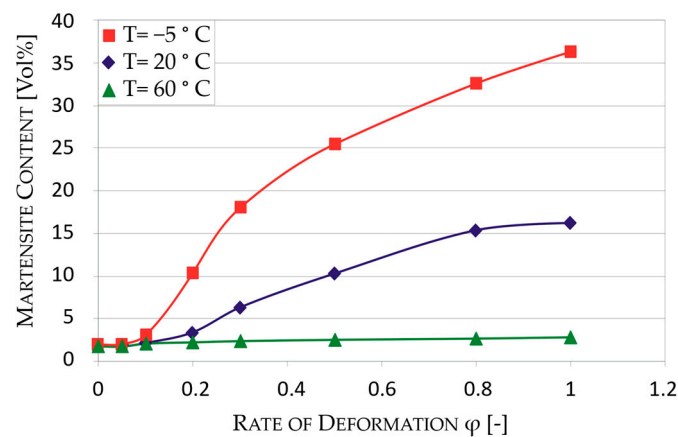

Figure 2. Martensite content in compression specimens (1.4301) as a function of forming temperature and degree of deformation in compressed specimens (strain rate = 0.1 1/s).

The deformation-induced martensite formation and the associated expression of the yield stress of a metastable austenitic CrNi steel are complex mechanisms that are largely determined by alloy components, the deformation parameters, and the temperature, as well as stress and strain state. There are a lot of publications describing the fundamental effects of phase transformation in metastable austenitic steels [12–14]. Specifically, in the field of forging, only a few research papers are known in which the effect of deformation-induced phase transformation and its applications are investigated [15,16].

In the past, several theses were written at the Bergakademie Freiberg, the subject of which was the occurrence of martensitic phases due to mechanical stress on the components close to the operation [17,18]. Currently, within the framework of the CRC 799 "TRIP-Matrix Composite", metastable austenitic CrMnNi cast steels with TRIP effect are being investigated [19].

At the University of Kaiserslautern, the influence of near-operational isothermal and thermal–mechanical stresses on the deformation behavior of metastable austenitic steels is investigated in the project "Influence of low temperatures on the cyclic deformation and transformation behavior of differently processed metastable austenites" as part of the Research Group "Engineering Materials on Different Scales: Experiment, Modelling and Simulation" [20].

In general, innovative solutions, especially in the field of manufacturing processes, aimed at improving certain aspects of a bearing have been a reoccurring topic in recent times. Extensive research has been done in the field of additive manufacturing, where one approach was to add a stainless steel layer to a base of less valuable steel, which leads to a hybrid steel–steel component. Also, the effects of treating stainless steel with a solution in order to make it more durable and therefore more suitable for bearing applications have been investigated [21].

Additionally, a topic that has not yet been investigated is the addition of rolling to the process presented in this paper. As Pape et al. [6,22] showed, the process of rolling can have a beneficial influence on bearing performance, and its application to the findings presented in this paper is part of ongoing research.

1.2. Roller Bearings

Bearings enable relative movement of machine parts and thus represent the concrete shape of joints in the sense of gear theory. Bearings take on both load-bearing and -guiding tasks. The "carrying" function focuses on transmitting forces and moments between parts that are moving relative to each other. Depending on the direction of the forces to be

transmitted, a distinction can be made between radial, axial and angular contact bearings. The "guide" function determines the relative position of the parts that are moving relative to each other as precisely as possible. Non-locating bearings are used for guidance in the radial direction, fixed bearings additionally or exclusively for axial determination [23].

The relative motion between the active surfaces of a bearing can be sliding or spinning (tangential), rolling (radial) or a combination. In roller bearings, the combination of (micro)sliding and rolling motion is very commonly observed. For angular contact ball bearings, all three components have to be considered. Sliding movements of solid-state surfaces in direct contact require a comparatively high amount of force and energy. At the same time, particles can detach, leading to surface wear during operation. This results in an essential requirement for a machine element: the function must be ensured or fulfilled for as long as possible. This means that destruction or progressive damage resulting in the eventual failure of the active surfaces or active bodies and an immediate or gradual change in the geometry with impairment of the guiding properties must be avoided or delayed for as long as possible. Typical mechanisms that can lead to functional impairment are breakage, plastic deformation, melting, seizure, fatigue, surface breakdown and wear [23].

In addition to adhesive and abrasive wear in conjunction with tangential relative movements and friction under unfavorable operating and lubrication conditions, surface fatigue is a common cause of failure of rolling bearing systems. Increasing the reliability of rolling bearing assemblies by avoiding early failures as well as increasing bearing life are therefore the main concerns in the development of rolling bearings. As a result of improved bearing designs, they can not only achieve a longer bearing life but can also be used in smaller, lighter, and low-friction designs with the same service life. Kloos and Broszeit define surface fatigue as "the separation of microscopic and macroscopic material particles (...) caused by fatigue cracking, crack progression and residual fracture during the rolling of two force-bound surfaces (with and without slippage) under certain mechanical, thermal and chemical stress conditions" [24]. In contrast to wear, surface fatigue is a typical form of damage caused by material chipping instead of the removal of the material. Wear and surface fatigue are system properties of a component pairing, while general fatigue is a component property. In this work angular contact ball bearings were used (Figure 3). These bearings allow radial and axial loading, but in addition to rolling also experience spinning motion with additional tangential shear forces. Most damage occurs at the inner ring, as it is the part of a bearing that sees the highest loads. Therefore, the inner ring was the part that was manufactured with the aforementioned process. For testing, the inner ring (Figure 3) was combined with a bought-in outer ring and balls.
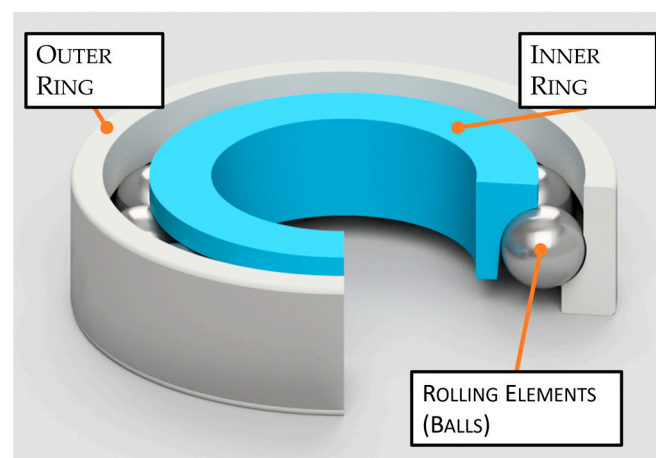

Figure 3. Cross section of an angular contact ball bearing, with the inner ring highlighted.

2. Material and Experimental Procedure

2.1. Material

For the forming of the inner rings the stainless steel 1.4301 (X5CrNi18-10) was used. This is a metastable austenitic stainless steel. The base material was first formed at low temperatures and then machine milled to obtain the outer dimensions of a bearing inner ring. The surface was not polished, which led to a rougher surface. The details of the manufacturing process are described in [25].

2.2. Test Rig Development and Bearing Performance Tests

At the IMKT, a novel test rig has been constructed on the foundational structure of a preexisting SKF-manufactured machine designed for radial loading (Figure 4). This upgraded test rig boasts the capability to concurrently test four bearings across two test heads. With a total of four machines featuring this configuration, a maximum capacity of testing up to 16 bearings simultaneously has been achieved. The two test heads were both connected to a central main shaft, interconnecting each unit's secondary shaft via hydraulic couplings.
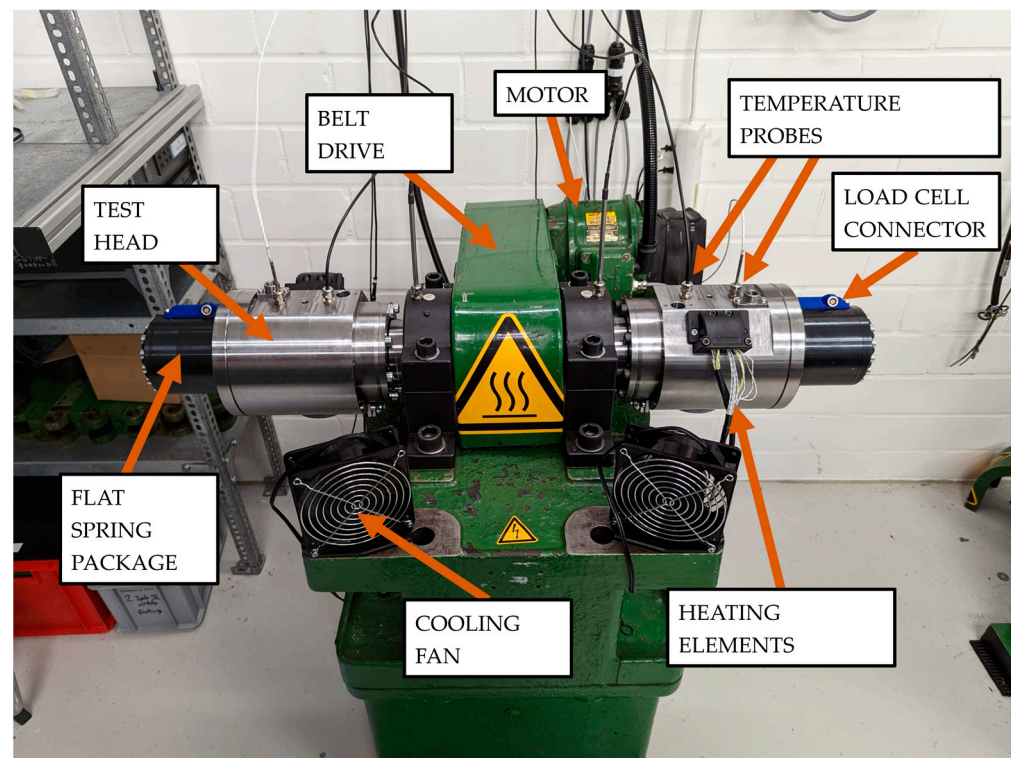

Figure 4. Angular contact ball bearing test rig.

The support mechanism for the test heads involves radial suspension utilizing a rod, with provision for attachment of a force sensor to measure the friction torque exhibited by a pair of bearings. Furthermore, the axial load was applied through a set of flat springs situated on the outermost periphery of the test head. This applied force was monitored using a load sensor, ensuring precise control and measurement during testing procedures. A cross section of the test head is shown in Figure 5.
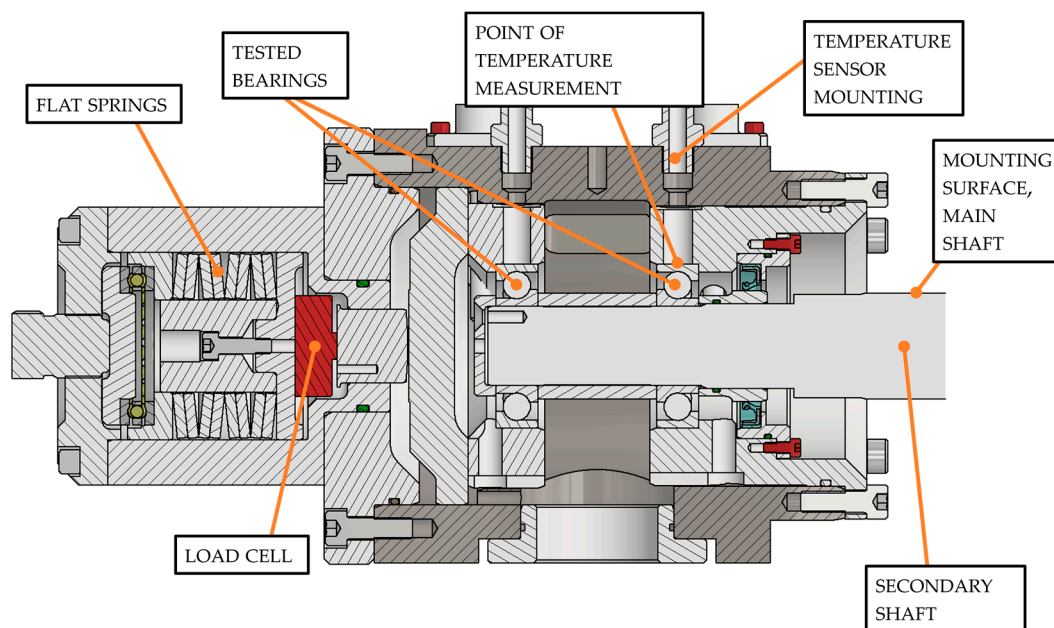
Figure 5. Cross section of a test head.

Each individual bearing within this setup was equipped with a temperature sensor positioned on its outer ring, enabling monitoring of thermal variations. Regrettably, due to spatial constraints, the installation of a temperature sensor on the inner ring of the bearing was deemed impractical and therefore not implemented.

The implementation of a free-floating support system for the test head was chosen for its simplicity and capabilities in regard to the measurement of friction torque, constituting a pivotal advantage. However, this advantageous setup introduces its own set of challenges, primarily revolving around the need for precise alignment during the installation phase. The precise alignment of the secondary shafts within the hydraulic couplings has been shown to be a critical factor, influencing especially the baseline vibrations recorded throughout the tests.

Moreover, the design decision for the free-floating support structure inherently subjects the bearings to radial loading, a factor demanding careful consideration. Evaluating the mass of the test head as approximately 38 kg allowed for an estimation of the radial loading exerted on each bearing, which could be conservatively estimated to reach 200 N or below. While this magnitude of radial loading warrants attention, preliminary calculations suggest that its impact on the anticipated life expectancy of the bearings appears negligible, with no discernible substantial influence identified through initial assessments.

In addition to the measured friction torque and temperature values, the condition monitoring of the bearings in the test was ensured by a vibration sensor system attached to the front of the test heads. With this, it was possible to detect any damage that formed in a timely manner.

2.3. Experimental Setup

When selecting the operating parameters for life expectancy tests, a critical consideration concerned the distinctive properties of the utilized materials. Given the limited knowledge regarding the fatigue limits of bearings made from austenitic steels, a pragmatic approach was applied to derive the operational parameters. Consequently, the outlined solution was proposed to address this challenge. The initial step involved identifying the limit for a standard bearing possessing identical outer dimensions, readily accessible through manufacturers' catalogues. A comparison of the material properties between bearing steel and austenitic steel revealed a notable reduction in the latter's capabilities. In the literature, the topic of bearing life for stainless steel bearings has not seen broad

attention. As such, for an initial estimate, the technical manual of the bearing manufacturer was consulted, where it was proposed that a reduction to 80% of the load applied on a bearing of same dimensions, but made from standard bearing steel, has been shown to be sufficient to ensure the stainless steel bearings can endure a similar runtime under load.

Consequently, a reduction in load was implemented to achieve a comparable fatigue life using the following approach.

For the standard 7206 bearings, operating within a Hertzian pressure limit of approximately 2.2 GPa and subjected to an axial load of 17,500 N, the maximum capacity of stainless steel bearings was conservatively estimated at 80% of that of the standard 100 Cr6. Given the recognized lower hardness of 1.4301 in its austenitic state, a further reduction in the load by an additional 5% was undertaken. This factor of 5% is assumed in a first step and can be adapted in future research. Therefore, the axial load for the series can be written as:

$$F_a = 17500 \times 0.75 \cong 13\text{kN}$$

Another important point for the operating conditions is the thickness of the lubrication film and the state of lubrication. The parameter that was considered was the specific height of the lubricating film Λ, which could be calculated from the roughness of the two contacting surfaces and the calculated minimal film height.

$$\Lambda = \frac{h_{min}}{\sqrt{R_{q,2}^2 + R_{q,1}^2}}$$

However, it is important to add that the measurement of the initial surface state of the bought-in variants could only be determined on a small number of exemplary units. It was not possible to reliably disassemble the bearings without damaging them. Therefore, a small number of randomly chosen bearings were pulled from the test pool and investigated for their surface structure beforehand. As those numbers showed little deviation from one other, the obtained values were taken as the initial state of all. An overview of the test parameters is given in Table 1.

Table 1. Overview test parameters.

Type	Speed (1/min)	Load (kN)	Temperature (°C)	Rq, Inner Ring	hMin (mm)	Lambda
Standard	2000	17.5	60	0.05	0.136	1.92
1.4301 cold-formed	2000	13	60	1.68	0.194	0.115
Industry-standard stainless	2000	13	60	0.4	0.194	0.481
1.4301 untreated	2000	13	60	1.7	0.194	0.114

In the test cycle, the bearings were lubricated using grease for high-speed applications. This specialized grease was selected to accommodate the relatively low load used in this test regimen.

3. Results

The bearings were investigated after manufacturing and compared to industrial stainless steel bearings. For this, the surface of the manufactured bearings had to be machined after the forging process. In the next step, the bearings were mounted into the test rig and fatigue tests were executed. In cased of surface failure or fatigue, the test was stopped. After the test, the bearings' surfaces were inspected by microscopy.

3.1. Hardness

The assessment of a bearing surface's hardness is a pivotal determinant in evaluating its suitability for bearing applications. Traditionally, standard bearing steel demonstrates

exceptional hardness, often surpassing the 1000 HV0.1 threshold. This elevated hardness level significantly exceeds the typical hardness achievable in various stainless steel counterparts. The steel under scrutiny in this research exhibited a base hardness measuring around 250 HV0.1. However, through lowering of the forming temperature, a substantial enhancement in its hardness to approximately 500 HV0.1 was achieved, as depicted in Figures 6 and 7. For investigations of the achievable hardness, the forming process was performed at −15 °C and −196 °C. With the cold forging process at −15 °C, a significant increase in surface hardness was achieved in comparison to the standard process. This was even able to be improved for the forging process conducted at −196 °C. This increase in hardness presents an intriguing avenue for optimizing its performance and applicability in bearing scenarios, underscoring the pivotal role of temperature modulation in altering the material's mechanical properties for enhanced functionality.
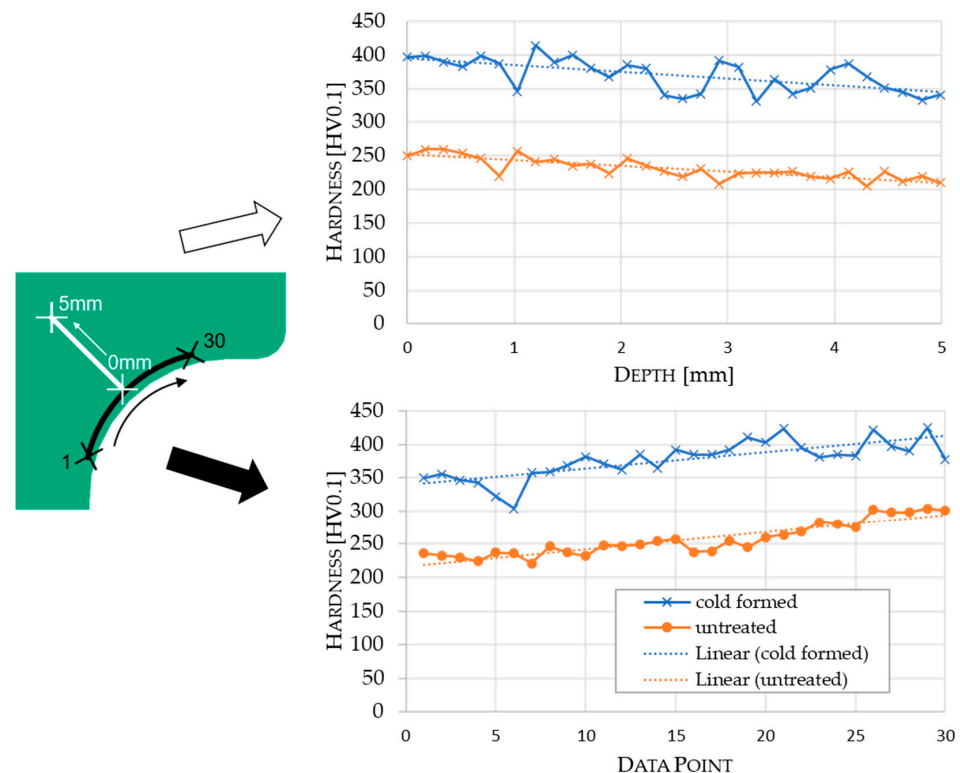

Figure 6. Hardness comparison between a cold-formed (at −15 °C) and a machined inner ring made from 1.4301.

Hardness was measured in two different directions on the different samples. Both were defined on the run zone. The depth direction started in the middle of the run zone and followed the angle of contact of the bearing, which per design was 40 degrees. The second direction followed the contour of the raceway outwards, with the beginning and the end approximately 1 mm outside of the run zone. Figure 6 shows that the hardness declined slightly more in the depth of the tested cold-formed specimen compared to the unaltered sample. In comparison to the untreated sample, significantly greater variations in hardness levels were evident in both dimensions. This can be likely attributed to the lack of homogeneity in the crystal lattice due to the produced martensite. Along the running zone, the trends in both samples were very similar. Additionally, besides the noticeably increased hardness, a more pronounced deviation from the mean was discernible compared to the initial material.
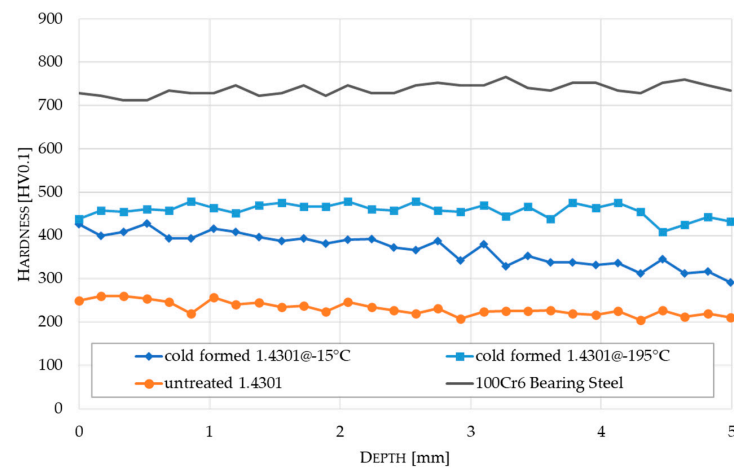
Figure 7. Hardness in increasing depth from surface: comparison between different forming temperatures and materials.

3.2. Roughness

Surface roughness has a strong impact on bearing life regarding mechanical performance and longevity. Surface roughness directly affects the tribological interactions within a bearing system, governing the contact between rolling elements and races. Excessive roughness can intensify abrasive wear, generating elevated frictional forces and accelerating material fatigue. In contrast, an excessively smooth surface might compromise the formation of crucial lubricating films, leading to inadequate separation between contacting surfaces and heightened risk of adhesive wear. The roughness of the contacting surfaces impacts load distribution, fatigue resistance, and overall operational reliability of bearings, thereby directly influencing their expected lifespan and performance under operational conditions.

The preliminary examination of surface characteristics, considering the previously outlined limitations, revealed that the cold-formed bearings exhibited a marginally rougher surface compared to the standard bearings (see Figure 8). For the standard bearings, the average posttest surface roughness was notably lower. However, it was crucial to note that the deviation in roughness was higher for the standard bearings. Both sets of bearings underwent a process of surface smoothening during testing, with the cold-formed bearings displaying a more pronounced effect. An important observation was that the initial state of the cold-formed bearings tended to be slightly rougher, attributable to the manufacturing process. In contrast, the standard bearings commenced with a comparatively smoother initial surface.
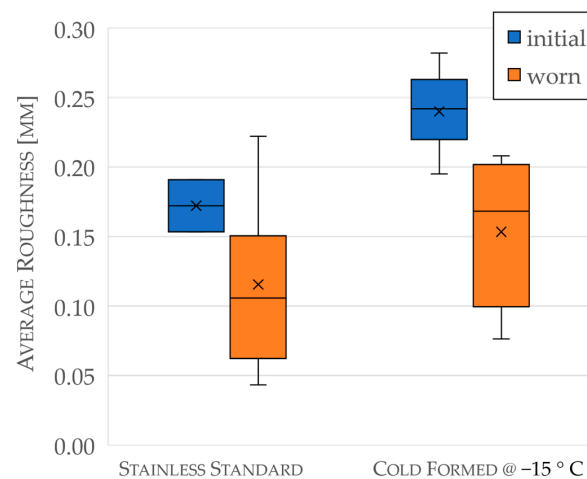

Figure 8. Comparison of the average roughness between two different bearing materials pre- and posttest.

3.3. Test Evaluation

Table 2 summarizes the results from a series of eight tests conducted on bearings subjected to 13 kN axial loading at 2000 rpm, while none ran more than 46 million cycles. The observed outcomes varied. Most tests saw noticeable signs of wear (V). Some showed extended pitting damage (P), characterized by broken up surfaces and signs of fracturing running along the sides of the pitting, as seen in Figure 9 (right-hand side. Three bearings showed a form of adhesive damage (A), characterized by a gray surface often accompanied by smaller pitting. Three bearings showed signs of overheating (H), especially characterized by dark discolored raceways. The tests were mostly terminated by the condition monitoring system watching over the vibrations (S). Two were ended by exceeding the temperature limit (T). One of those tests was most probably not sufficiently lubricated and therefore taken out of consideration (not counted).

Table 2. Overview of tested standard bearings (sets of 2).

Test#	Load Cycles (mio.)	Inner Bearing Damage	Outer Bearing Damage	End of Test (Reason)	Counted
1	4.46	A	V	S	1
2	17.98	A	V	S	1
3	46.00	V, A	V	S	1
4	2.36	P	A, (P)	S	1
5	5.99	-	H	T	0
6	19.18	-	V, P	S	1
7	35.96	V, H, P	V	T	1
8	31.17	V, H	V	S	1

Figure 9. Example of standard bearing damage.

A microscopic image of an industrial stainless steel bearing after test in shown in Figure 9. The red arrow indicates the direction in which the rollers moved along the surface. The bearing run for over 250 h, and the test stopped due to bearing damage. In the visual examination of the worn stainless steel bearing, distinct characteristics indicative of prolonged use and stress concentrations were apparent. Notably, the run zone exhibited considerable darkening, suggesting heightened frictional forces and localized overheating during operation. Concurrently, a number of small pits manifested prominently within the region experiencing the highest pressure, as can be seen in the microscope image on the right. These discernible pits underscore the consequential effects of repetitive loading, potentially indicating surface fatigue and material degradation in response to the intense mechanical stresses endured by the bearing during its operational life cycle.

The results from the series of cold-formed bearings can be seen in Table 3. Overall, there were 10 tests conducted with two bearings per test. The conditions for speed, load, temperature, and lubrication were the same as in previous series. One set was retracted in the early stages of the testing and could not be tested again. This was due to a sensor error that led to us being unable to determine the faulty bearing on this particular test rig. As the conditions may be altered by the mounting process, we decided to retract both sets of bearings, although one set was unharmed (tests 3 + 4). One set was later damaged during the mounting process and was never used.

Table 3. Overview of tested cold-formed bearings (sets of 2).

Test#	Load Cycles (mio.)	Inner Bearing Damage	Outer Bearing Damage	End of Test Reason	Counted
1	132.35	-	P, A	S	1
2	10.90	P	V	S	1
3	0.72	-	-	-	0
4	0.72	A	P	S	1
5	115.08	V, A	(P)	S	1
6	112.82	V	H	T	1
7	0	M	M	-	0
8	84.49	V, A	V	S	1
9	342.48	V	V	X	1
10	4.63	V	V, H, P(!)	S	1

As in the previous array of tests, the most common observation was signs of wear (V). The occurrence of overheated surfaces (H) was less common, and also in the two instances that showed discoloring, less pronounced. On the other hand, the fatigue damage occurrences had a much larger affected area than on the standard bearings. This could be a sign of faster rupture of the surface layers, as the detection method was the same. Therefore, a newly formed pitting would be growing more slowly on the standard bearing surface than in the cold-formed bearings. This could be due to the formation of martensite being sometimes inhomogeneous, which could then lead to larger pieces breaking out of the surface in cases where a sufficient crack was formed under the surface.

A cold-formed stainless steel bearing inner ring after a test of only 0.72 million cycles is shown in Figure 10. The bearing showed a large pitting defect, spanning the entire width of the contact zone, with nearly the same length in the circumferential direction. Furthermore, an additional facet of the visual assessment revealed a polished character in the contact area, due to wear, which was often observed in these bearings.

Figure 10. Example for cold-formed bearing damage.

3.4. Bearing Life

We can show that the process significantly improves bearing life. A direct comparison of industrial stainless steel bearings and the manufactured bearings is shown in the Weibull plot (Figure 11). By the beneficial martensitic surface with increased hardness, the bearing fatigue was increased by a factor of approximately 2. This featured a significant effect and allowed for improved machine elements. The results also proved that due to the highest loads on the bearings' inner ring, only this part suffered fatigue and was the critical part.
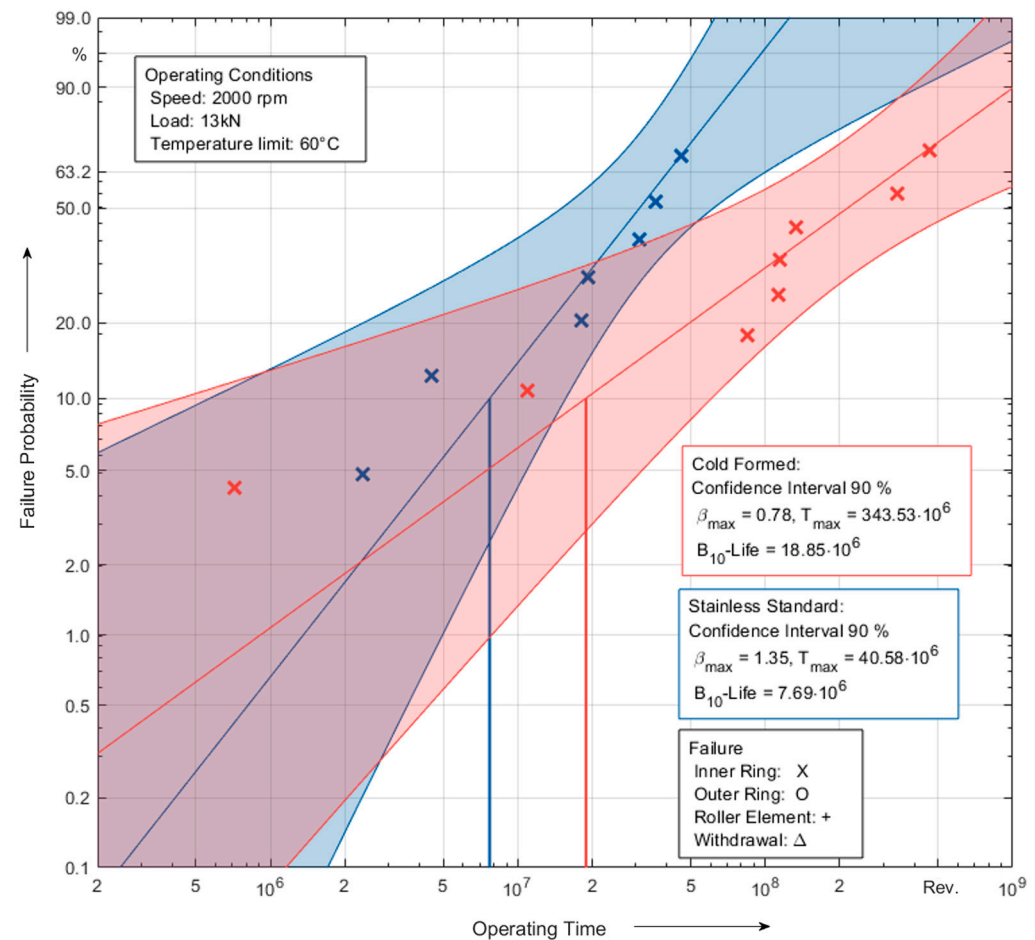

Figure 11. Weibull plot for industrial stainless steel bearings in comparison to bearings with induced martensitic phase.

4. Conclusions

Stainless steel bearings often serve as essential components within machinery. However, their current state is often subjected to fatigue due to a comparatively small surface hardness. Addressing this concern, the proposed method aimed at enhancing the surface integrity of stainless steel bearings through a low-temperature forging technique, demonstrating a significant augmentation in bearing fatigue life. This enhancement stems from the creation of a martensitic subsurface layer characterized by increased surface hardness.

An essential consequence of this process involved the induction of beneficial residual stresses attributed to martensite formation. While the forging process posed considerable challenges, particularly concerning radial bearings, its application to axial bearings proved relatively straightforward. This simplicity not only fosters improved machine elements but also enables the construction of more compact, resource-efficient facilities.

Consequently, future studies will center on the low-temperature forging of axial bearing washers to induce a martensitic subsurface, thereby potentially replicating the success witnessed in other bearing components. The integration of such a forging technique into

bearing fabrication appears relatively seamless. Despite the incremental energy expenditure for cooling during this process, it is substantially offset by the substantial increase in bearing fatigue life—a trade-off that amplifies the overall durability and reliability of these critical machine components.

Author Contributions: Investigation, A.H.B.; Resources, G.P.; Writing—original draft, A.H.B.; Writing—review & editing, F.P.; Supervision, F.P. and G.P.; Project administration, G.P.; Funding acquisition, G.P. All authors have read and agreed to the published version of the manuscript.

References

1. Coors, T.; Mildebrath, M.; Büdenbender, C.; Saure, F.; Faqiri, M.Y.; Kahra, C.; Prasanthan, V.; Chugreeva, A.; Matthias, T.; Budde, L.; et al. Investigations on Tailored Forming of AISI 52100 as Rolling Bearing Raceway. *Metals* **2020**, *10*, 1363. [CrossRef]
2. Pape, F.; Coors, T.; Barroi, A.; Hermsdorf, J.; Mildebrath, M.; Hassel, T.; Kaierle, S.; Matthias, T.; Chugreev, A.; Chugreeva, A.; et al. Tribological Study on Tailored-Formed Axial Bearing Washers. *Tribol. Online* **2018**, *13*, 320–326. [CrossRef]
3. Voskamp, A.P.; Mittemeijer, E.J. State of residual stress induced by cyclic rolling contact loading. *Mater. Sci. Technol.* **1997**, *13*, 430–438. [CrossRef]
4. Voskamp, A.P. Ermüdung und Werkstoffverhalten im Wälzkontakt. *HTM J. Heat Treat. Mater.* **1998**, *53*, 25–30. [CrossRef]
5. Voskamp, A.P. Microstructural stability and bearing performance. In *Bearing Steel Technology*; ASTM International: West Conshohocken, PA, USA, 2022.
6. Denkena, B.; Poll, G.; Maiß, O.; Pape, F.; Neubauer, T. Enhanced boundary zone rolling contact fatigue strength through hybrid machining by hard turn-rolling. *Bear. World J.* **2016**, *1*, 87–102.
7. Bhadeshia, H.K.D.H. Steels for bearings. *Prog. Mater. Sci.* **2012**, *57*, 268–435. [CrossRef]
8. Noury, P.; Eriksson, K. Failures of high strength stainless steel bridge roller bearings: A review. *Eng. Fract. Mech.* **2017**, *180*, 315–329. [CrossRef]
9. Chen, H.; Zeng, T.; Shi, Q.; Wang, N.; Zhang, S.; Yang, K.; Yan, W.; Wang, W. Microstructure Evolution and Mechanical Properties during Long-term Tempering of a Low Carbon Martensitic Stainless Bearing Steel. *J. Mater. Res. Technol.* **2023**, *25*, 297–309. [CrossRef]
10. Schmidt, W.; Küppers, W. Der Einfluß der Austenit-Stabilität auf mechanische Eigenschaften und Umformverhalten von Chrom-Nickel-Stählen, Thyssen Edelstahl. *Tech. Berichte 12* **1986**, *1*, 80–100.
11. Barenbrock, D. Einfluss Verformungsinduzierter Martensitumwandlung Auf das Rissfortschrittsverhalten Austenitischer Stähle. Ph.D. Dissertation, Universität Hannover, Hannover, Germany, 2002.
12. Olsen, G.B.; Cohen, M. Kinetics of strain induced martensite nucleation. *Met. Trans A* **1975**, *6*, 791–795. [CrossRef]
13. Lindenberg, H.-U.; Kazmierski, O.; Otto, A. Kaltgewalztes Band aus nichtrostenden Edelstählen und die Anwendungspotentiale. *Stahl. Und. Eisen.* **2000**, *5*, 37–42.
14. Schmitz, K.W. Beitrag zum Tiefziehen von Unterschiedlich Stabil Austenitischen Werkstoffen bei Gezielter Temperaturführung. Ph.D. Dissertation, TU Clausthal, Clausthal-Zellerfeld, Germany, 1974.
15. Biermann, H.; Christos, A. *Austenitic TRIP/TWIP Steels and Steel-Zirconia Composites Design of Tough, Transformation-Strengthened Composites and Structures: Design of Tough, Transformation-Strengthened Composites and Structures*; Springer: Cham, Switzerland, 2020. [CrossRef]
16. Henschel, S.; Posselt, F.; Dudczig, S.; Wetzig, T.; Aneziris, C.G.; Krüger, L. Experimental determination of toughness under mode I/II loading. *Procedia Struct. Integr.* **2020**, *28*, 1369–1377. [CrossRef]
17. Onyuna, M.O. Deformation Behaviour and Martensitic Transformations in Metastable Austenitic Steels and Low Alloyed Multiphase Steels. Ph.D. Dissertation, Bergakademie Freiberg, Freiberg, Germany, 2003.
18. Schoß, V. Martensitische Umwandlung und Ermüdung Austenitischer Edelstähle, Gefügeveränderungen und Möglichkeiten der Früherkennung von Ermüdungs-Schädigungen. Ph.D. Dissertation, Bergakademie Freiberg, Freiberg, Germany, 2001.
19. Oettel, H.; Martin, U. The nature of the TRIP-effect in metastable austenitic steels. *Int. J. Mater. Res.* **2006**, *97*, 1642–1647. [CrossRef]
20. Beck, T.; Smaga, M. Influence of the Surface State on Quasi-static and Cyclic Deformation and Damage Behavior of TRIP/TWIP Steels (B10), DFG-Project 172116086. Available online: https://gepris.dfg.de/gepris/projekt/278735173 (accessed on 1 February 2024).

21. Zheng, K.; Zhong, Z.; Wang, H.; Xu, H.; Yu, F.; Wang, C.; Wu, G.; Liang, J.; Godfrey, A.; Cao, W. Obtaining Excellent Mechanical Properties in an Ultrahigh-Strength Stainless Bearing Steel via Solution Treatment. *Metals* **2023**, *13*, 1824. [CrossRef]
22. Pape, F.; Terwey, J.T.; Maiss, O.; Li, X. Editorial: Rolling bearing optimization through innovative manufacturing processes. *Front. Manuf. Technol.* **2024**, *3*, 1352187. [CrossRef]
23. Steinhilper, W.; Sauer, B. *Konstruktionselemente des Maschinenbaus 2, Grundlagen von Maschinenelementen für Antriebsaufgaben*, 6th ed.; Springer: Berlin/Heidelberg, Germany, 2008.
24. Kloos, K.H.; Broszeit, E. Grundsätzliche Betrachtungen zur Oberflächenermüdung. *Werkstofftechnik* **1976**, *3*, 85–96. [CrossRef]
25. Behrens, B.A.; Brunotte, K.; Wester, H.; Peddinghausen, J.; Till, M. Functionalisation of the Boundary Layer by Deformation-Induced Martensite on Bearing Rings by means of Bulk Metal Forming Processes. In Proceedings of the 31st International Conference on Metallurgy and Materials, METAL 2022, Brno, Czech Republic, 18–19 May 2022; pp. 250–255.